



HAL
open science

Spin-Valley Coupling Anisotropy and Noise in CMOS Quantum Dots

Cameron Spence, Bruna Cardoso Paz, Bernhard Klemt, Emmanuel Chanrion, David Niegemann, Baptiste Jadot, Vivien Thiney, Benoit Bertrand, Heimanu Niebojewski, Pierre-André Mortemousque, et al.

► **To cite this version:**

Cameron Spence, Bruna Cardoso Paz, Bernhard Klemt, Emmanuel Chanrion, David Niegemann, et al.. Spin-Valley Coupling Anisotropy and Noise in CMOS Quantum Dots. *Physical Review Applied*, 2022, 17 (3), pp.034047. 10.1103/PhysRevApplied.17.034047 . hal-03749553

HAL Id: hal-03749553

<https://hal.science/hal-03749553>

Submitted on 25 Aug 2023

HAL is a multi-disciplinary open access archive for the deposit and dissemination of scientific research documents, whether they are published or not. The documents may come from teaching and research institutions in France or abroad, or from public or private research centers.

L'archive ouverte pluridisciplinaire **HAL**, est destinée au dépôt et à la diffusion de documents scientifiques de niveau recherche, publiés ou non, émanant des établissements d'enseignement et de recherche français ou étrangers, des laboratoires publics ou privés.


Spin-Valley Coupling Anisotropy and Noise in CMOS Quantum Dots

Cameron Spence,^{1,*} Bruna Cardoso Paz¹,¹ Bernhard Klemt,¹ Emmanuel Chanrion¹,¹ David J. Niegemann¹,¹ Baptiste Jadot¹,¹ Vivien Thiney,¹ Benoit Bertrand²,² Heimanu Niebojewski,² Pierre-André Mortemousque,² Xavier Jehl,³ Romain Maurand,³ Silvano De Franceschi³,³ Maud Vinet,² Franck Balestro,¹ Christopher Bäuerle,¹ Yann-Michel Niquet,³ Tristan Meunier,¹ and Matias Urdampilleta^{1,†}

¹ *Université Grenoble Alpes, CNRS, Grenoble INP, Institut Néel, Grenoble 38402, France*

² *CEA, LETI, Minatec Campus, Grenoble F-38054, France*

³ *Université Grenoble Alpes, CEA, IRIG, Grenoble 38000, France*

 (Received 11 October 2021; revised 13 December 2021; accepted 1 March 2022; published 16 March 2022)

One of the main advantages of silicon spin qubits over other solid-state qubits is their inherent scalability and compatibility with the 300-mm complementary metal oxide semiconductor (CMOS) fabrication technology that is already widely used in the semiconductor industry, while maintaining high readout and gate fidelities. We demonstrate the detection of a single electron spin using energy-selective readout in a CMOS-fabricated nanowire device with an integrated charge detector. We measure a valley splitting of 0.3 meV and 0.16 meV in two similar devices. The anisotropy of the spin-valley mixing is measured and shown to follow the dependence expected from the symmetry of the local confinement, indicating low disorder in the region of the quantum dot. Finally the charge noise in the strong spin-valley coupling regime is investigated and found to induce fluctuations in the qubit energy in the range of 0.6 GHz/ $\sqrt{\text{Hz}}$.

DOI: [10.1103/PhysRevApplied.17.034047](https://doi.org/10.1103/PhysRevApplied.17.034047)

I. INTRODUCTION

Silicon spin qubits are a highly promising candidate for scalable quantum computation. High-fidelity spin measurement with integrated charge sensing up to relatively high temperature, fast electron spin resonance or electric dipole spin resonance manipulation for one- and two-qubit gates, and long coherence times in isotopically purified silicon all point toward the high potential of the silicon platform for solid-state qubit [1–5]. Additionally, industrial foundries dedicated to complementary metal oxide semiconductor (CMOS) fabrication provide a clear path toward mass production of low-variability qubit devices [6,7]. At the same time, exploiting microelectronic potential offers the possibility to cointegrate classical and quantum hardware which is a key requirement for performing large-scale quantum operations in solid state. In this context, spin readout and manipulation have been demonstrated in foundry-fabricated CMOS quantum dots with high fidelity [8–11]. However, characterization of the spin physics in these types of devices remains an open problem, with indications of local disorder and variability across similar devices [12].

In this paper we present the measurement of spin relaxation in CMOS quantum dots fabricated on a foundry-compatible 300-mm wafer. We first show how we can rapidly probe the spin using an energy-selective readout with more than 90% readout fidelity. Secondly, we explore the dynamics of spin relaxation in the system and the coupling of spin and valley states, by measuring the spin lifetime as a function of magnetic field strength and direction. Finally, we investigate the charge noise in this system by performing spin-valley relaxometry.

The three devices we present here have the same geometry as the one depicted in Fig. 1(a). They consist of a pair of split front gates, of length 50 nm and separated by 50 nm, lying on a silicon nanowire of width 90 nm and thickness 15 nm. Two electron reservoirs are formed by ion implantation for the first device and *in situ* growth of degenerate *n*-doped silicon for the other ones. They have been measured at low temperature, between 100 and 350 mK. At this temperature, a quantum dot is formed under each front gate, G_1 and G_2 , in the corners of the nanowire. We operate the device as follows: the quantum dot QD1 under G_1 is used to trap a single charge and QD2 under G_2 is operated in the many-electron regime to form a single-electron transistor (SET). Figure 1(b) shows the stability diagram with respect to V_{G1} , V_{G2} . Shifts in the Coulomb peaks indicate it is possible to detect the first electron entering QD1, using the SET. When QD1 is depleted to the few-electron

*cameron.spence@neel.cnrs.fr

†matias.urdampilleta@neel.cnrs.fr

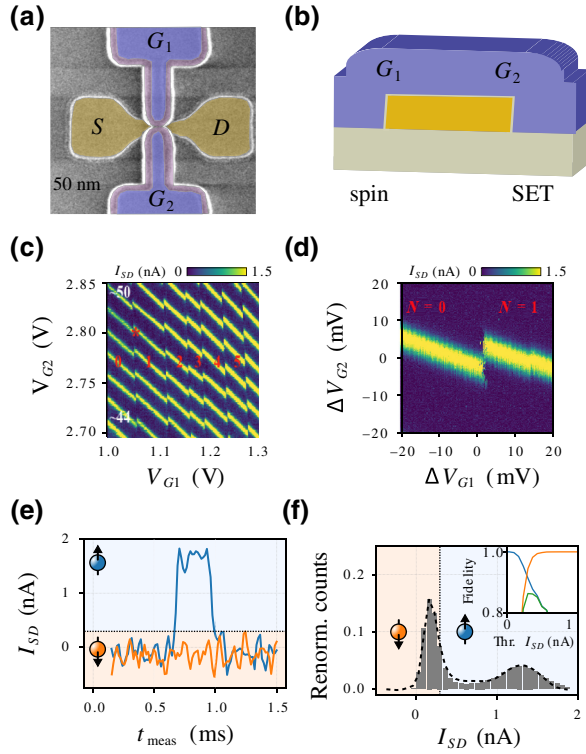


FIG. 1. (a) Schematic of a CMOS-fabricated nanowire-type device identical in structure to the devices used here. The silicon channel (yellow) connects two electron reservoirs labeled *S* and *D*. Two front gates, G_1 and G_2 , which are isolated from the channel by 6 nm of SiO_2 and 5 nm of TiN, control the chemical potential of quantum dots formed in the corner of the Si nanowire. A metallic top gate is positioned 400 nm above the channel and is biased to +2 V. Finally, the silicon bulk below the buried oxide is polarized and used as a back gate (+5 V). (b) Schematic cross section of the device. The quantum dots are localized in the corners of the silicon nanowire. The one under G_2 is operated in the single-electron transistor regime to charge-sense the single electron under G_1 . (c) Stability diagram of the two quantum dots when QD2 is operated as a SET ($N_e > 30e^-$) to probe QD1 charge occupancy. The bright regions of current correspond to Coulomb peaks where transport is possible through the SET under G_2 . The addition of an electron to QD1 causes a shift in the potential of the SET, indicated by the sharp cut. (d) Enlarged stability diagram of the first electron transition for QD1. (e) Representative time traces of the source drain current through the SET I_{SD} during spin measurement. If a spin-up electron is loaded, it is able to rapidly tunnel out of the dot, causing a transient shift in the sensor current as the dot is briefly emptied, indicated in blue. If a spin-down electron is loaded, it remains in the qubit dot and the sensor current does not change, indicated in orange. A threshold current I_{thr} is defined to distinguish between the two states. (f) State fidelity analysis at an optimized measurement point. A histogram of the maximum current of more than 1000 measurements is binned. The black dashed line is the total distribution obtained from simulation of more than 10 000 sample traces using experimental parameters. Inset: The individual state fidelity is calculated for varying threshold current level, with $F(|\uparrow\rangle)$ in blue and $F(|\downarrow\rangle)$ in orange. The product of these, the state visibility V , is plotted in green.

regime, the current passes only through the SET. We operate the device at the transition signaling the addition of the first electron in QD1.

II. SINGLE-SHOT READOUT OF A SINGLE ELECTRON SPIN

To read out the spin state, we exploit a spin-to-charge conversion based on energy-selective tunneling [13]. For this purpose, at finite magnetic field, we first load QD1 with a single electron and then pulse the chemical potential where only the highest spin state can tunnel out of the dot. Therefore, when the electron is in an up spin state, we observe a signal click, characteristic of the tunneling out of an up spin electron, followed by the tunneling in of a down spin electron, depicted in Fig. 1(c) (blue curve). In contrast, for a spin down, the signal is constant. It is important to note that similarly to Ref. [13], in all three devices, the loading and unloading of the single spin is achieved through the SET and not through the reservoir. This single-shot detection of the spin state is further analyzed by setting the detection threshold at the point of maximum visibility. To find this point, we build the histogram presented in Fig. 1(d) where we bin the maximum of each measurement trace which lasts for 1 ms with a sampling rate at 50 kHz. The visibility is obtained by using the same method as in Ref. [13], which involves simulating single-shot traces using the extracted tunneling-in and tunneling-out times (250 μs and 411 μs , respectively) to describe the current distribution. We obtain an average readout fidelity above 92% (and 86% visibility) limited by the tunneling-in and tunneling-out rates of the single electron [14].

III. SPIN-VALLEY COUPLING

We now move on to the characterization of relaxation time. Relaxation curves are measured by first loading an electron with random spin orientation, and then probing the spin-up population after a given waiting time in the loading region. We obtain the curve in Fig. 2(a), which is characteristic of spin relaxation and presents a T_1 of 10 ms.

A. Determination of valley splitting

To further investigate the presence of excited states, we measure the relaxation rate as a function of the magnetic field on the two devices. Figure 2 present the results obtained on three devices (blue, red, and green data points). The three curves feature a hotspot in relaxation at different magnetic fields (0.5 T, 1.6 T, and 2.6 T). At these points, the two valley states with opposite spins anticross (the valley splitting E_{VS} is equal to the Zeeman splitting E_Z) and give rise to a relaxation channel through spin-valley mixing [15].

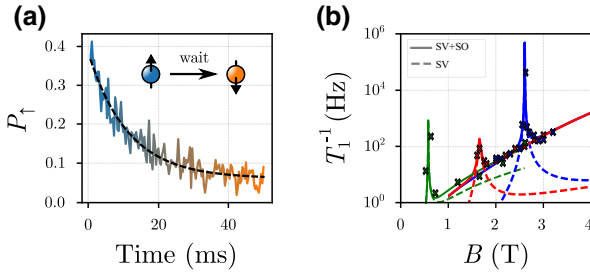


FIG. 2. (a) Spin-up population during measurement as a function of the waiting time after loading. It is fitted with an exponential decay function to extract T_1 , the spin relaxation time. (b) The average relaxation rate T_1^{-1} for three similar devices is plotted as a function of the magnetic field orthogonal to the nanowire axis. It is fitted (solid line) with a combination of the spin-valley contribution Γ_{SV} (dashed line) and the spin-orbit contributions Γ_{SO} to the relaxation rate. A single prominent increase of relaxation rate, occurring at 0.5 T, 1.7 T, and 2.6 T, is induced by spin-valley mixing close to $E_z = E_{SV}$ and coupling to the phonon bath. Outside of this hotspot, the spin relaxation is induced by spin-orbit mixing with higher orbital states.

To support this interpretation we fit the data points with a model comprising spin-orbit and spin-valley contributions [15,16],

$$T_1^{-1} = \Gamma_{\text{Ph,SV}} + \Gamma_{\text{JN,SO}} + \Gamma_{\text{Ph,SO}}, \quad (1)$$

which is represented by solid lines. Here $\Gamma_{\text{Ph,SV}}$ corresponds to the relaxation rate due to spin-valley mixing and coupling to phonons, while $\Gamma_{\text{Ph,SO}}$ and $\Gamma_{\text{JN,SO}}$ correspond to the relaxation rates due to spin-orbit coupling via phonons and Johnson-Nyquist noise, respectively. From these fits we obtain a valley splitting energy, E_{VS} , of $62 \pm 7 \mu\text{eV}$, $191 \pm 16 \mu\text{eV}$, and $300 \pm 13 \mu\text{eV}$, respectively, and a gap at the spin-valley anticrossing of $0.3 \pm 0.05 \mu\text{eV}$, $4 \pm 0.3 \mu\text{eV}$, and $0.2 \pm 0.03 \mu\text{eV}$, respectively. The effect of Johnson-Nyquist noise on the spin-valley contribution has been neglected as at the hotspots the density of phonon modes is high enough to dominate the relaxation process. The $\Gamma_{\text{Ph,SV}}$ contribution is therefore represented by the dashed curves which are in good agreement with the experimental data around the hotspot. The spin-orbit contribution (baseline) follows in all cases a similar model which accounts for Johnson-Nyquist noise at low field (where the density of phonons is small) and phonon emission at higher field [17]. Interestingly, the three devices present the same relaxation rates outside the hotspots. This indicates that the overall structure of the quantum dots is similar in all three devices, indicating that the disorder at quantum dot scale is small. This is an important result toward the realization of reliable and low-variability quantum dots when operated far from the hotspot.

B. Anisotropic spin-valley mixing

Spin-valley mixing provides an excellent probe of the local symmetry of the quantum dot [12,16,18,19]. It is indeed expected that spin-valley mixing vanishes in the presence of more than one mirror plane in the structure [9]. The presence of a hotspot is already the sign of a lower symmetry of the system. The present quantum dots are formed in the corner of the nanowire, and therefore, in the absence of local disorder, we expect a single mirror plane with its normal vector along x , the nanowire axis.

To probe the presence of local disorder, we investigate the anisotropic behavior of spin-valley mixing. Such measurements can be used to determine the direction of the spin-orbit contribution which can be directly correlated to the local planes of symmetry experienced by the quantum dot. Figures 3(a)–3(c) presents the measurement of the relaxation rate as the field direction is rotated in three different orthogonal planes. To achieve the maximum sensitivity, the magnitude of the magnetic field is set close to the hotspot where the relaxation rate is dominated by spin-valley mixing (2.4 T). When the magnetic field scans the XZ and YZ plane, we observe a drop in the relaxation rate when it crosses the x axis. In contrast, the relaxation rate is constant in the YZ plane.

To interpret these data, we need to consider the spin-orbit coupling Hamiltonian H_{SOC} that couples the spin and v_1, v_2 valley orbitals through the spin-valley mixing

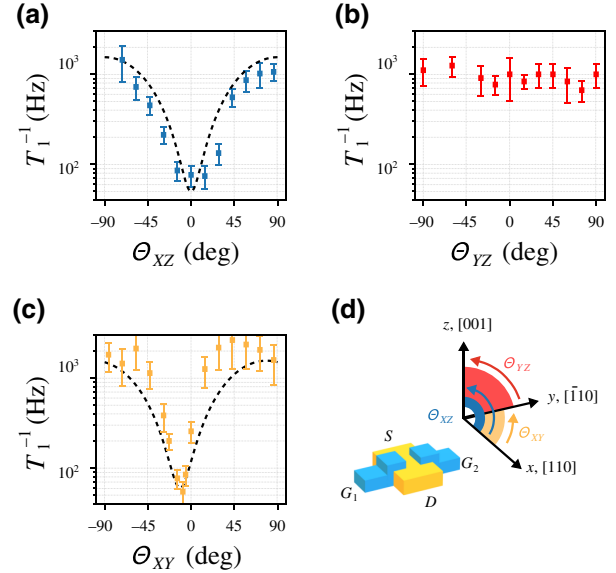


FIG. 3. Evolution of the relaxation rate with rotation of the magnetic field. (a)–(c) Evolution of the relaxation rate within the XZ (XY , YZ) plane [under rotation about the y (z , x) axis, corresponding approximately to the $[\bar{1}10]$ ($[001]$, $[110]$) crystallographic axis]. Dashed curves in (a),(b) correspond to \sin^2 functions fitted to the data. (d) Schematic representation of the device and its spatial orientation.

matrix element $\langle v_1 \uparrow | H_{\text{SOC}} | v_2 \downarrow \rangle$ [20]. In the presence of a (yz) mirror-symmetry plane H_{SOC} takes the form $H_{\text{SOC}} = (\alpha_y p_y + \alpha_z p_z) \sigma_x + (\beta_y \sigma_y + \beta_z \sigma_z) p_x$, with p_x , p_y , and p_z the electron momentum in the x , y , and z directions and σ_x , σ_y , σ_z the Pauli matrices. The valley orbitals v_1 and v_2 being invariant by the (yz) mirror plane, $\langle v_1 | p_x | v_2 \rangle = \langle v_1 | -p_x | v_2 \rangle = 0$; see the Supplemental Material [12]. Therefore the spin mixing term reads $\langle v_1 \uparrow | (\alpha_y p_y + \alpha_z p_z) \cdot \sigma_x | v_2 \downarrow \rangle$. When the magnetic field is aligned with x , $|\uparrow\rangle$ and $|\downarrow\rangle$ are eigenstates of σ_x , which leads to a vanishing spin-valley mixing. As the magnetic field is tilted away from x at an angle θ , the remaining projection leads to $|\langle v_1 \uparrow | H_{\text{SOC}} | v_2 \downarrow \rangle|^2 \propto \sin^2 \theta$ [9,16]. Following this model, we obtain quantitative agreement between the experimental data and the \sin^2 function as shown in Figs. 3(a) and 3(b). From these fits, we obtain the minimum relaxation rate along the nanowire axis ([110]); see the diagram in Fig. 3(d). Along this axis, the relaxation is dominated only by the spin-orbit interaction. It is important to note that there is a slight offset in the angle in the XY measurement because the nanowire axis is not perfectly aligned with the coil axes. Moreover, the small discrepancy between the XY and XZ measurements suggests that Y and Z directions are not equivalent. This second-order anisotropy can be explained by the overlap of the front gate being nonequivalent between the side and the top facets of the wire.

IV. LOW-FREQUENCY CHARGE NOISE ON VALLEY SPLITTING

Valley splitting is sensitive to the electric field as it arises from the strong confinement against the top interface [21]. Here, we use the relaxation at the hotspot to probe the local fluctuations in electric field induced by low-frequency charge noise. For this purpose, we sit at a measurement point next to the hotspot and record the evolution of T_1 with time. To transform this time evolution into a power spectral density for E_{VS} , we assume that the dependence of the valley splitting on the electric field is linear for small noise amplitude [22]. From the hotspot fitting we extract the gradient at the measurement point, which, combined with a Fourier transform of the time-domain signal, Fig. 4(a), yields the power spectral density (PSD) in Fig. 4(b).

The PSD follows a $1/f$ dependence which, extrapolated to 1 Hz, gives $23 \mu\text{eV}^2/\text{Hz}$. In terms of qubit energy fluctuations, the value obtained is relatively large if we consider the operation of the qubit in a spin-valley mode. In this mode, the spin-valley mixing is exploited to drive coherent oscillations through electric dipole spin resonance next to the hotspot [20]. Fluctuations of the valley splitting translate into fluctuations of the Larmor frequency $\hbar \delta f = 1/2 \delta E_{\text{VS}}$ at the hotspot. This corresponds to a fluctuation in the spin precession of about $0.6 \text{ GHz}/\sqrt{\text{Hz}}$, which is faster

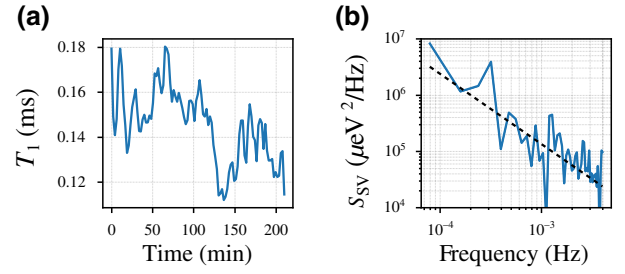


FIG. 4. (a) Variation in the spin-lattice relaxation rate over time. Each measurement point represents a T_1 measurement of duration 4 min. (b) Frequency-domain fluctuations of the valley splitting energy E_{VS} . The fit is proportional to $1/f^{1.25}$. Extrapolation to 1 Hz reveals fluctuations in E_{VS} of $23 \pm 1 \mu\text{eV}^2/\text{Hz}$.

than the decoherence rate due to the hyperfine fluctuations in natural silicon, and is of the order of the decoherence rate of charge and valley qubits [23,24]. This could prove detrimental for electric dipole spin resonance exploiting the spin-valley mode, limiting the coherence time when the spin-valley coupling is turned on [25,26]. It may therefore be necessary to operate further away from the hotspot to avoid fast decoherence, at the cost of slower Rabi frequency or to lower the confinement potential to reduce the valley splitting sensitivity to electric field [20]. It is worth noting that such a qubit experiment could not be achieved in the present device due to too low a spin-valley coupling at the low-field hotspot ($0.3 \pm 0.05 \mu\text{eV}$).

V. CONCLUSION

In conclusion, we have demonstrated fast and reproducible spin characterization in CMOS nanowire devices. A similar spin-orbit-induced relaxation rate was found across three identically patterned and fabricated devices, which is an important result toward the improvement of the CMOS fabrication process at the quantum dot level. Moreover, the spin-valley coupling was found to be highly anisotropic, with a strong symmetry plane oriented perpendicular to the channel axis, indicating the absence of strong local disorder at the quantum dot site. These results are of prime importance as they have been obtained in devices fabricated in a 300-mm foundry, which could ensure production of a large number of quantum dots with low variability, a requirement to go to large scale. Finally, low-frequency fluctuations in the valley splitting were measured to cause fluctuations in the Larmor frequency at $0.6 \text{ GHz}/\sqrt{\text{Hz}}$ which would be detrimental to the operation of the qubit as a spin-valley or valley qubit to enhance Rabi frequencies. This motivates further work on dependence and sensitivity of the valley splitting with respect to the electric field and the investigation of potential sweetspot.

ACKNOWLEDGMENTS

We acknowledge fruitful discussions with E. Bonet, J. Li, and L. Hutin and support from P. Perrier, H. Rodeñas, E. Eyraud, D. Lepoittevin, I. Pheng, T. Crozes, L. Del Rey, D. Dufeu, J. Jarreau, J. Minet, and C. Guttin. D.J.N., B.K., and C.S. acknowledge the GreQuE doctoral programs (Grant No. 754303). The device fabrication is funded through the QuCube project (Grant No. 810504). This work is supported by the Agence Nationale de la Recherche through the CRYMCO and MAQSi projects (ANR-20-CE24-9 and ANR-18-CE47-7).

-
- [1] J. Yoneda, K. Takeda, T. Otsuka, T. Nakajima, M. Delbecq, G. Allison, T. Honda, T. Kodera, S. Oda, and Y. Hoshi, *et al.*, A quantum-dot spin qubit with coherence limited by charge noise and fidelity higher than 99.9%, *Nat. Nanotech.* **13**, 102 (2018).
- [2] A. West, B. Hensen, A. Jouan, T. Tanttu, C. H. Yang, A. Rossi, M. F. Gonzalez-Zalba, F. E. Hudson, A. Morello, D. J. Reilly, and A. S. Dzurak, Gate-based single-shot readout of spins in silicon, *Nat. Nanotechnol.* **14**, 437 (2019).
- [3] M. Veldhorst, C. H. Yang, J. C. C. Hwang, W. Huang, J. P. Dehollain, J. T. Muhonen, S. Simmons, A. Laucht, F. E. Hudson, K. M. Itoh, A. Morello, and A. S. Dzurak, A two-qubit logic gate in silicon, *Nature* **526**, 410 (2015).
- [4] W. Huang, C. H. Yang, K. W. Chan, T. Tanttu, B. Hensen, R. C. C. Leon, M. A. Fogarty, J. C. C. Hwang, F. E. Hudson, K. M. Itoh, A. Morello, A. Laucht, and A. S. Dzurak, Fidelity benchmarks for two-qubit gates in silicon, *Nature* **569**, 532 (2019).
- [5] J. Y. Huang, W. H. Lim, R. C. C. Leon, C. H. Yang, F. E. Hudson, C. C. Escott, A. Saraiva, A. S. Dzurak, and A. Laucht, A high-sensitivity charge sensor for silicon qubits above 1 K, *Nano Lett.* **21**, 6328 (2021).
- [6] M. Veldhorst, H. G. J. Eenink, C. H. Yang, and A. S. Dzurak, Silicon cmos architecture for a spin-based quantum computer, *Nat. Commun.* **8**, 1766 (2017).
- [7] S. Schaal, A. Rossi, V. N. Ciriano-Tejel, T.-Y. Yang, S. Barraud, J. J. L. Morton, and M. F. Gonzalez-Zalba, A CMOS dynamic random access architecture for radio-frequency readout of quantum devices, *Nat. Electron.* **2**, 236 (2019).
- [8] M. Urdampilleta, D. J. Niegemann, E. Chanrion, B. Jadot, C. Spence, P.-A. Mortemousque, C. Bäuerle, L. Hutin, B. Bertrand, S. Barraud, R. Maurand, M. Sanquer, X. Jehl, S. DeFranceschi, M. Vinet, and T. Meunier, Gate-based high fidelity spin readout in a CMOS device, *Nat. Nanotechnol.* **14**, 737 (2019).
- [9] A. Corna, L. Bourdet, R. Maurand, A. Crippa, D. Kotekar-Patil, H. Bohoslavskyi, R. Laviéville, L. Hutin, S. Barraud, X. Jehl, M. Vinet, S. De Franceschi, Y.-M. Niquet, and M. Sanquer, Electrically driven electron spin resonance mediated by spin–valley–orbit coupling in a silicon quantum dot, *NPJ Quantum Inf.* **4**, 6791 (2018).
- [10] R. Maurand, X. Jehl, D. Kotekar-Patil, A. Corna, H. Bohoslavskyi, R. Laviéville, L. Hutin, S. Barraud, M. Vinet, M. Sanquer, and S. De Franceschi, A CMOS silicon spin qubit, *Nat. Commun.* **7**, 13575 (2016).
- [11] A. Crippa, R. Ezzouch, A. Aprá, A. Amisse, R. Laviéville, L. Hutin, B. Bertrand, M. Vinet, M. Urdampilleta, T. Meunier, M. Sanquer, X. Jehl, R. Maurand, and S. De Franceschi, Gate-reflectometry dispersive readout and coherent control of a spin qubit in silicon, *Nat. Commun.* **10**, 2776 (2019).
- [12] V. N. Ciriano-Tejel, M. A. Fogarty, S. Schaal, L. Hutin, B. Bertrand, L. Ibberson, M. F. Gonzalez-Zalba, J. Li, Y.-M. Niquet, M. Vinet, and J. J. L. Morton, Spin readout of a CMOS quantum dot by gate reflectometry and spin-dependent tunnelling, *PRX Quantum* **2**, 010353 (2021).
- [13] A. Morello, J. J. Pla, F. A. Zwanenburg, K. W. Chan, K. Y. Tan, H. Huebl, M. Möttönen, C. D. Nugroho, C. Yang, J. A. Van Donkelaar, A. D. C. Alves, D. N. Jamieson, C. C. Escott, L. C. L. Hollenberg, R. G. Clark, and A. S. Dzurak, Single-shot readout of an electron spin in silicon, *Nature* **467**, 687 (2010).
- [14] D. Keith, S. K. Gorman, L. Kranz, Y. He, J. G. Keizer, M. A. Broome, and M. Y. Simmons, Benchmarking high fidelity single-shot readout of semiconductor qubits, *New J. Phys.* **21**, 063011 (2019).
- [15] P. Huang and X. Hu, Spin relaxation in a Si quantum dot due to spin-valley mixing, *Phys. Rev. B* **90**, 235315 (2014).
- [16] X. Zhang, R.-Z. Hu, H.-O. Li, F.-M. Jing, Y. Zhou, R.-L. Ma, M. Ni, G. Luo, G. Cao, G.-L. Wang, X. Hu, H.-W. Jiang, G.-C. Guo, and G.-P. Guo, Giant Anisotropy of Spin Relaxation and Spin-Valley Mixing in a Silicon Quantum dot, *Phys. Rev. Lett.* **124**, 257 (2020).
- [17] P. Huang and X. Hu, Electron spin relaxation due to charge noise, *Phys. Rev. B* **89**, 195302 (2014).
- [18] A. Hofmann, V. F. Maisi, T. Krähenmann, C. Reichl, W. Wegscheider, K. Ensslin, and T. Ihn, Anisotropy and Suppression of Spin-Orbit Interaction in a GaAs Double Quantum dot, *Phys. Rev. Lett.* **119**, 176807 (2017).
- [19] T. Tanttu, B. Hensen, K. W. Chan, C. H. Yang, W. W. Huang, M. Fogarty, F. Hudson, K. Itoh, D. Culcer, A. Laucht, A. Morello, and A. S. Dzurak, Controlling Spin-Orbit Interactions in Silicon Quantum Dots Using Magnetic Field Direction, *Phys. Rev. X* **9**, 021028 (2019).
- [20] L. Bourdet and Y.-M. Niquet, All-electrical manipulation of silicon spin qubits with tunable spin-valley mixing, *Phys. Rev. B* **97**, 155433 (2018).
- [21] T. Struck, A. Hollmann, F. Schauer, O. Fedorets, A. Schmidbauer, K. Sawano, H. Riemann, N. V. Abrosimov, L. Cywiński, D. Bougeard, and L. R. Schreiber, Low-frequency spin qubit energy splitting noise in highly purified $^{28}\text{Si}/\text{SiGe}$, *NPJ Quantum Inf.* **6**, 20 (2020).
- [22] D. J. Ibberson, L. Bourdet, J. C. Abadillo-Uriel, I. Ahmed, S. Barraud, M. J. Calderón, Y.-M. Niquet, and M. F. Gonzalez-Zalba, Electric-field tuning of the valley splitting in silicon corner dots, *Appl. Phys. Lett.* **113**, 053104 (2018).
- [23] D. Kim, D. R. Ward, C. B. Simmons, J. K. Gamble, R. Blume-Kohout, E. Nielsen, D. E. Savage, M. G. Lagally, M. Friesen, S. N. Coppersmith, and M. A. Eriksson, Microwave-driven coherent operation of a semiconductor

- quantum dot charge qubit, [Nat. Nanotechnol.](#) **10**, 243 (2015).
- [24] N. E. Penthorn, J. S. Schoenfield, J. D. Rooney, L. F. Edge, and H. W. Jiang, Two-axis quantum control of a fast valley qubit in silicon, [NPJ Quantum Inf.](#) **5**, 94 (2019).
- [25] D. Culcer, A. L. Saraiva, B. Koiller, X. Hu, and S. Das Sarma, Valley-Based Noise-Resistant Quantum Computation Using Si Quantum Dots, [Phys. Rev. Lett.](#) **108**, 126 (2012).
- [26] C. H. Yang, A. Rossi, R. Ruskov, N. S. Lai, F. A. Mohiyaddin, S. Lee, C. Tahan, G. Klimeck, A. Morello, and A. S. Dzurak, Spin-valley lifetimes in a silicon quantum dot with tunable valley splitting, [Nat. Commun.](#) **4**, 2069 (2013).